# Acoustic valley edge states in a graphene-like system with sub-wavelength resonator

Heng Jiang, Meng Chen, Yu Liu, Tao Yang, Wenshuai Xu, Yihan Liu, Mangong Zhang, and Yuren Wang

Citation: The Journal of the Acoustical Society of America **146**, 736 (2019); doi: 10.1121/1.5115016
View online: https://doi.org/10.1121/1.5115016
View Table of Contents: https://asa.scitation.org/toc/jas/146/1
Published by the Acoustical Society of America



# Acoustic valley edge states in a graphene-like system with sub-wavelength resonator

Heng Jiang,[1,a)] Meng Chen,[1,a)] Yu Liu,[1,a)] Tao Yang,[1,a)] Wenshuai Xu,[1,a)] Yihan Liu,[2] Mangong Zhang,[3] and Yuren Wang[1,b)]

[1]*Key Laboratory of Microgravity, Institute of Mechanics, Chinese Academy of Sciences, Beijing 100190, People's Republic of China*

[2]*Petrochina Oil and Gas Pipeline Control Center, Beijing 100007, People's Republic of China*

[3]*Wuhan Second Ship Design and Research Institute, Wuhan, Hubei 430064, People's Republic of China*

(Received 10 January 2019; revised 20 April 2019; accepted 25 April 2019; published online 31 July 2019)

Recently, the study of topological phase transitions and edge states for acoustic wave systems has become a research hotspot. However, most current studies on topological edge states are based on Bragg scattering, which is not practical to apply in situations involving low-frequency sound because of the large structural dimensions. Therefore, the authors construct, in this study, a graphene-like structure based on a sub-wavelength resonant unit Helmholtz resonator and adjust the acoustic capacitance diameter of adjacent units to change the local resonance frequency, and thereby impose the degeneracy of the Dirac cone and topological spin states, which is characterized by valley Chern numbers of opposite sign. The authors also check topological valley edge states at zigzag and armchair interfaces and find that gapless topological valley edge states only appear at zigzag interfaces, whereas armchair interfaces host gap edge states. Moreover, the results show that the transmission properties of edge states in a zigzag rectangular waveguide are immune to backscattering and defects.  https://doi.org/10.1121/1.5115016

[RF] Pages: 736–741

## I. INTRODUCTION

In recent years, the development of the quantum Hall effect (Klitzing, 1986; Laughlin, 1983), quantum spin Hall effect (Kane and Mele, 2005; Bernevig *et al.*, 2006), and topological insulators (Hasan and Kane, 2010; Qi and Zhang, 2011) in condensed-matter physics has inspired the study of topological phase transitions and edge states for classical wave systems such as phononic crystals (Wang *et al.*, 2009; Khanikaev *et al.*, 2012; Hafezi *et al.*, 2013; Rechtsman *et al.*, 2013). As with electronic materials, these classical wave systems can be used to make bandgap structures by designing artificial periodic structures, but they belong to the class of bosonic systems and have no obvious response to external magnetic fields considering the spin effect. Meanwhile, the linear acoustic wave equation remains invariant under time reversal, so it cannot be simply analogous to spin degeneracy. To solve this problem, researchers implemented the acoustic analogous quantum Hall effect (Miniaci *et al.*, 2018; Mousavi *et al.*, 2015), Floquent topological insulators, and topological edge states in acoustic systems by introducing a circulating background airflow (similar to the effect of magnetic field) (Fleury *et al.*, 2014; Ni *et al.*, 2016; Yang *et al.*, 2015), time-space modulation (Fleury *et al.*, 2016; Khanikaev *et al.*, 2015; Peng *et al.*, 2016; Souslov *et al.*, 2017), and coupling resonance (He *et al.*, 2016; Wei *et al.*, 2017). Furthermore, researchers implemented phononic analogs of the quantum spin Hall effect and topological boundary states by constructing a lattice structure with a specific symmetry, which creates a sonic pseudospin state by breaking space-inversion symmetry (He *et al.*, 2015). This method of breaking space-inversion symmetry to implement an acoustic topological phase is simple, practical, and very promising for the development of topological acoustics.

Constructing acoustic topological systems by breaking space-inversion symmetry involves two key steps: first, constructing a lattice structure with the requisite symmetry to create a Dirac cone at the high-symmetry points of the Brillouin zone and, second, making the Dirac cone degenerate by breaking the space-inversion symmetry. Currently, acoustic topological systems are constructed mainly by arranging scatterers in a triangular or hexagonal lattice, thereby forming a Dirac cone at the high symmetry K point or at the center of the Brillouin zone (Lu *et al.*, 2017; Zhang *et al.*, 2017a). In addition, a Dirac-like cone forms at the center of the square lattice (Huang *et al.*, 2011). The main ways to break the spatial symmetry include changing the filling ratio (Zhang *et al.*, 2017a), executing a rotation operation (Lu *et al.*, 2016), or changing the geometric parameters (Zhang *et al.*, 2017b) so as to reduce the symmetry of the entire system. Liu *et al.* inverted *p*/*d* symmetrical bands by adjusting the filling ratio and designed an "*x*-type" splitter to study the chiral propagation characteristic of acoustic topological boundary states (He *et al.*, 2015). Numerous studies have focused on the triangular or hexagonal lattices arranged by non-cylindrical scatterers and have used rotation to reduce spatial symmetry, and thereby construct the quantum pseudospin Hall effect and topological edge states. In

[a)]Also at: University of Chinese Academy of Sciences, Beijing, 100049, People's Republic of China.

[b)]Also at: University of Chinese Academy of Sciences, Beijing, 100049, People's Republic of China. Electronic mail: yurenwang@imech.ac.cn

addition, researchers have also broken space-inversion symmetry by modulating the geometric parameters of the lattice elements in the graphene-like structure, to realize the boundary topological state of the acoustic wave (Lu *et al.*, 2016). However, most current studies on acoustic topological phase transitions and topological boundary states are based on Bragg scattering. The wavelength of the applied frequency is usually $0.5\lambda$, which typically requires a large geometric size to support low-frequency sound waves. Therefore, sub-wavelength units must be introduced into the acoustic topology structure to achieve acoustic topological phase transitions and boundary states at sub-wavelength scales (Yves *et al.*, 2017a; Yves *et al.*, 2017b) .

Helmholtz resonators and concentrated-mass locally resonant units have sub-wavelength resonators, and thereby allow effective control over long-wavelength sound waves (Fang *et al.*, 2006). Therefore, introducing these sub-wavelength locally resonant units into the design of topological acoustic systems is likely to solve the operational problems caused by low-frequency sound waves. However, poor impedance matching between concentrated-mass locally resonant units and the air leads to poor energy transmittance. Therefore, we construct in the present study a graphene-like structure by using a sub-wavelength resonant unit Helmholtz resonator and adjust the acoustic capacitance diameter of the adjacent units to change the local resonance frequency, and thereby make the Dirac cone degenerate with topological spin states. We demonstrate the existence of topological transitions by varying the radii of the two adjacent acoustic chambers; these transitions are characterized by valley Chern numbers of opposite sign. In addition, the valley-protected topological edge states are confirmed along the interfaces separating the topological insulators with opposite spin states.

## II. HELMHOLTZ ACOUSTIC METAMATERIAL STRUCTURE

Figure 1 shows the system structure of the Helmholtz resonators arranged in the form of a graphene-like lattice structure. The two adjacent lattice points A and B have different sound volume diameters, $R-\Delta r$ and $R+\Delta r$, respectively, and the height is H. The diameter of the sound path is $r$, the height is $H_2$, the waveguide width is W, and the height is $H_1$. When the diameters of A and B are equal, the entire structure has a $C_{3v}$ point group structure, which has triple mirror symmetry and triple rotational symmetry. When the diameters of A and B are not equal, the mirror symmetry of the entire structure is broken, and the system degrades from a $C_{3v}$ symmetry to a $C_3$ symmetry.

Employing the finite-element software COMSOL Multiphysics to calculate the band structure of the Helmholtz metamaterials, the calculation model was reduced to a single unit, as shown in Fig. 1(b), by applying Bloch boundary conditions on opposing boundaries. The entire band structure was obtained by sweeping the wave vector along the edges of the irreducible Brillouin zone. In the calculation, only the air was considered, with the following parameters: density $\rho = 1.25\,\mathrm{kg/m^3}$ and sound velocity $c = 343\,\mathrm{m/s}$. The geometric parameters of the metamaterials are as follows: lattice constant $a = 30\,\mathrm{mm}$, $R = 6.25\,\mathrm{mm}$, $H = 2\,\mathrm{mm}$ for the acoustic chamber, $r = 1\,\mathrm{mm}$, $H_2 = 1\,\mathrm{mm}$ for a short tube; $w = 6\,\mathrm{mm}$, and $H_1 = 3\,\mathrm{mm}$ for a wave guide.

Helmholtz resonant acoustic metamaterials can effectively reduce the frequency band structure and lead to sub-wavelength control of acoustic waves (Fang *et al.*, 2006). According to the design theory of the Helmholtz resonator, the short neck and the acoustic cavity of the Helmholtz resonator are regarded as the acoustic mass (similar to inductance in electronic circuits) and the acoustic capacitance (similar to capacitance in electronic circuits), respectively. Subject to external excitation, the air at the short neck of the Helmholtz resonator oscillates vertically, radiating sound waves into the surrounding medium. The resonance frequency is

$$f = \frac{1}{2\pi\sqrt{LC}}, \tag{1}$$

which is far less than the frequency corresponding to the wavelength of the sound wave. Moreover, the resonance

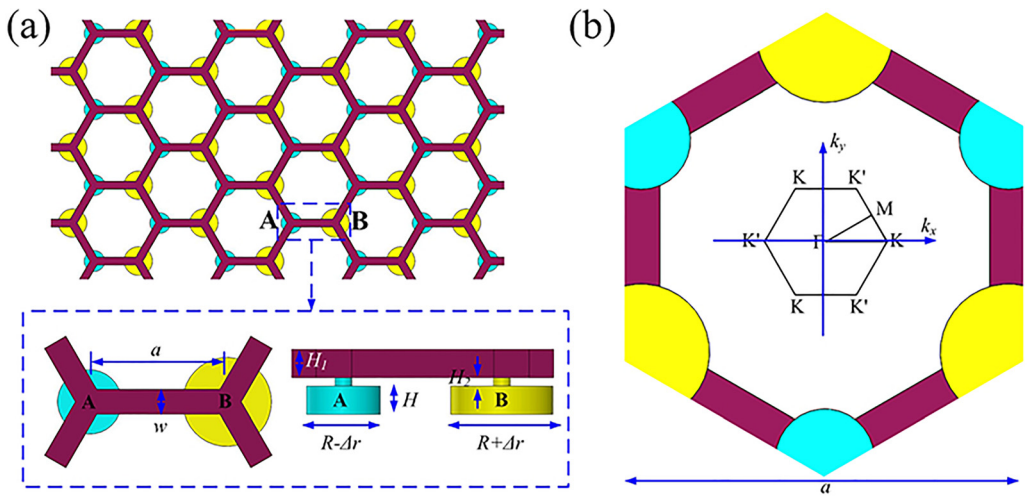


FIG. 1. (Color online) (a) Layout and (b) unit cell of Helmholtz acoustic metamaterial structure.

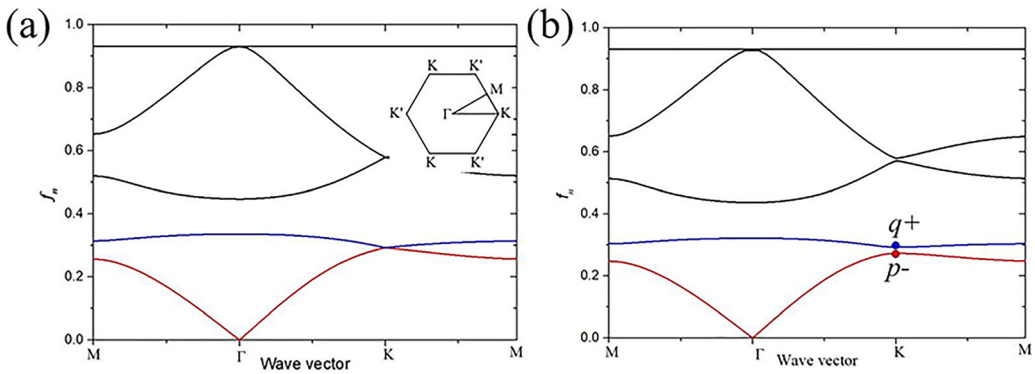


FIG. 2. (Color online) Bandgap structure and Dirac point of Helmholtz acoustic metamaterial structure. Calculated band structures with (a) $\Delta r = 0$ mm, and (b) $\Delta r = 0.25$ mm.

frequency may be tuned by adjusting the geometric parameters. This approach leads to a good design for subwavelength topological acoustic systems.

Figures 2(a) and 2(b) show the bulk band dispersion curves of the Helmholtz acoustic metamaterial structure with $\Delta r = 0$ mm and $\Delta r = 0.25$ mm, respectively. A subwavelength Dirac cone forms at the high-symmetry K point of the Brillouin zone at $\Delta r = 0$ mm, and its normalized frequency $\omega a/2\pi c$ is 0.2829 ($\omega/2\pi$ means that the actual physical frequency of the Dirac cone is 3205.7 Hz, $a$ is the lattice constant of 30 mm, and $c$ is the speed of sound propagating in air, 343 m/s). When the adjacent units in a Helmholtz acoustic superstructure have the same size, the entire system satisfies triple mirror symmetry and triple rotational symmetry. In other words, the lattice point group and the hexagonal lattice are consistent with $C_{3V}$ symmetry.

When $\Delta r = 0.25$ mm, the triple-mirror symmetry of the entire system is broken because of the unequal size of the resonator unit at the adjacent lattice point, which reduces the symmetry to $C_3$. Meanwhile, the sub-wavelength Dirac-cone degeneracy at the K point is lifted, which gives rise to a complete band gap with the normalized frequency of 0.2732–0.2930 (actual frequency is 3097–3320.1 Hz). At the K point, a pair of extreme frequency points form as $q^+$ (3097 Hz) and $p^-$ (3320.1 Hz) because of a degradation of the degeneracy. Furthermore, for the Helmholtz acoustic metamaterial structure, a Dirac cone also appears at $\omega a/2\pi c = 0.5$, which is due to Bragg scattering, and the corresponding frequency is greater.

## III. SUBWAVELENGTH ACOUSTIC VALLEY VORTEX

Figure 3 shows the variation of the frequency extremes with $\Delta r$ at the K point in the Brillouin zone. As the absolute value of $\Delta r$ increases, the local resonance frequencies between adjacent lattices differ more, causing the subwavelength band gap to gradually increase. When $\Delta r = 0$, the sub-wavelength band gap closes because of the symmetry at the K point, with $q^+$ and $p^-$ forming a degenerate state. As $\Delta r$ varies from $-3$ to 3 mm, the band gap near the subwavelength Dirac cone opens, closes, and then reopens. The insets in Fig. 3 shows the absolute sound pressure distribution at the extremes of the frequency for $\Delta r = -0.25$ mm and $\Delta r = 0.25$ mm. The valley states $q^+$ and $p^-$ have opposite vortex directions (at the lattice point of the hexagonal lattice). When $\Delta r = -0.25$ mm, $q^+$ at the upper cutoff frequency of the bandgap has clockwise chirality, whereas $p^-$ at the lower cutoff frequency of the band gap has anticlockwise chirality. When $\Delta r = 0.25$ mm, the energy band is reversed, and the valley states $q^+$ and $p^-$ exchange their spin states; that is, $q^+$ is located at the lower cutoff frequency of the band gap and $p^-$ is located at the upper cutoff frequency of the bandgap. The band structure of the Helmholtz acoustic metamaterial structure reverses with changes in the diameter of the adjacent lattice cavity, which stimulates the subwavelength topological phase transition and spin state.

To better understand this topological phase transitions, we introduce a nonzero valley Chern number. Through the $k \cdot p$ perturbation method, the topological phase transition can be described by the continuum Hamiltonian (Zhang *et al.*, 2017b):

$$H_K(\delta \boldsymbol{k}) = V_D \delta k_x \sigma_x + V_D \delta k_y \sigma_y + m V_D^2 \sigma_z, \tag{2}$$

where $V_D$ is the Dirac velocity of the conic dispersion at $\Delta r = 0$ mm, $\delta \boldsymbol{k}$ is the momentum deviation from the valley center $K$, and $\sigma_i$ are the Pauli matrices of the vortex pseudospins. The effective mass characterizes two different valley states with opposite vortices:

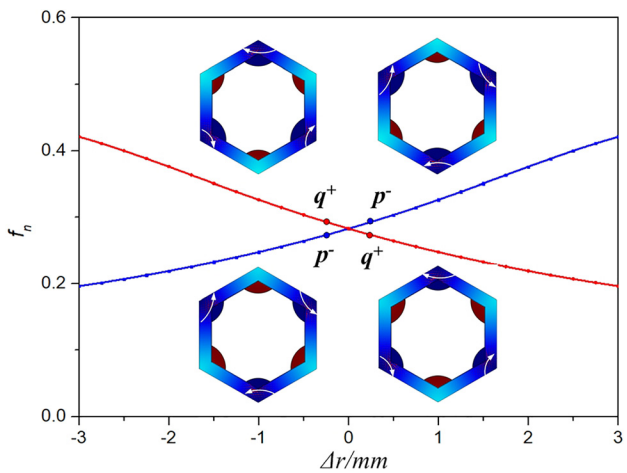


FIG. 3. (Color online) Band-edge frequencies depicted for acoustic system with different $\Delta r$. Color illustrations show the distribution of absolute sound pressure at the valley states $q^+$ and $p^-$ for $\Delta r = -0.25$ and $\Delta r = 0.25$.

$$m = \frac{\Delta\omega}{2V_D^2}, \tag{3}$$

where the bandwidth $\Delta w = w_{q+} - w_{p-}$, so the effective Hamiltonian depends strongly on $\Delta r$. The local Berry curvature $\Omega_k(\delta\boldsymbol{k})$ centered at the K valley can be calculated by using the eigenvector, and topological charges can be calculated by integrating the local Berry curvature (Semenoff *et al.*, 2008; Martin *et al.*, 2008; Qiao *et al.*, 2011):

$$C_k = \frac{1}{2\pi}\int \Omega_k(\delta\boldsymbol{k})ds = \frac{1}{2}\mathrm{sgn}(m). \tag{4}$$

The Chern number K′ can be derived from time-reversal symmetry and has the opposite sign. The valley Chern number is

$$C_v = C_k - C_{k'}. \tag{5}$$

With $\Delta r < 0$, the valley Chern number is nonzero 1, and the Chern number has the opposite sign for $\Delta r < 0$ because of the reversal of the sub-wavelength band gap. Thus, the topological phase transition occurs in conjunction with a change of the valley Chern number at $\Delta r = 0$ mm, which predicts that edge states propagate along the interface between the two hexagonal lattices with opposite $\Delta r$.

## IV. SUBWAVELENGTH TOPOLOGICAL VALLEY EDGE STATES

To prove the existence of sub-wavelength topological edge states at the interface, two types of superlattices are established for the cases $\Delta r = -0.25$ mm with six unit cells labeled N type and $\Delta r = 0.25$ mm with six unit cells labeled M type. Two types of N−M interfaces usually exist in graphene-like structures. One is the zigzag type [see Fig. 4(a)], and the other is the armchair type [see Fig. 4(b)]. The two calculated types of interface bandgap structures and edge state sound pressure distributions are shown in Figs. 5 and 6.

Figure 5 shows the bandgap structure of the zigzag-type interface, in which the red part is the scattering curve of the edge state and the black curves represent the dispersion curve of the bulk state. In the middle of the bandgap of the bulk state, at a frequency at which the acoustic wave cannot propagate, the topological phase transition exhibits a gap-free edge state at the interface. Figure 5(b) shows the sound-pressure distribution of the valley states K and K′. Since the Chern number changes by +1 at the valley state B ($k = 2a_0/3\pi$) from N to M, the edge state of the sound wave propagates rightward at this position, while the change of the Chern number is −1 at the valley state A ($k = -2a_0/3\pi$), so the edge state of sound waves propagates in the opposite direction. The valley pseudospin of the state is locked to the propagation direction. This means that each valley state corresponds to only one direction of propagation.

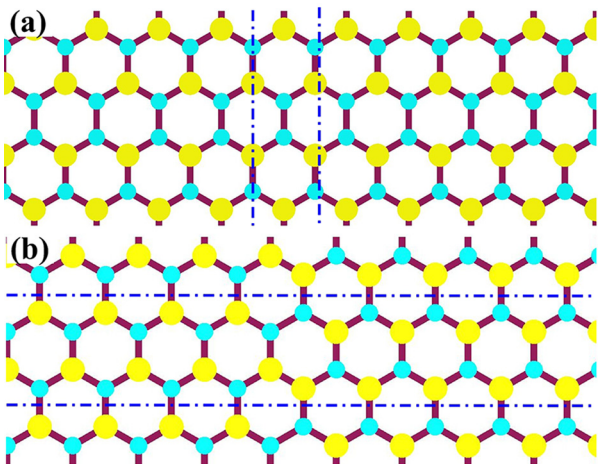


FIG. 4. (Color online) Two types of interfaces: (a) zigzag-type interface and (b) armchair-type interface.

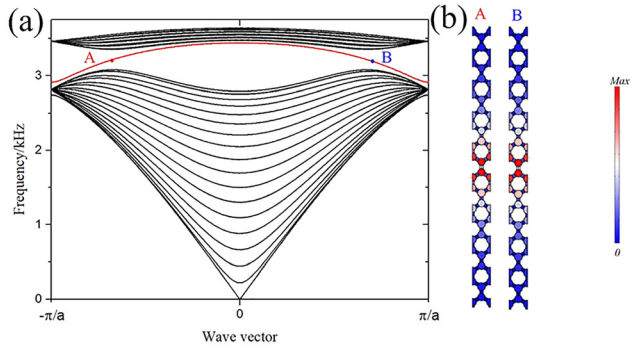


FIG. 5. (Color online) (a) Bandgap structure of zigzag-type interface, and (b) sound pressure distribution of valley states A and B.

## V. ANALYSIS OF ROBUSTNESS OF SUBWAVELENGTH TOPOLOGICAL VALLEY SPIN TRANSMISSION

A Z-shaped waveguide was first established to study the sub-wavelength topological valley spin transmission by 25 × 24 units, with all interfaces being zigzag-type interfaces,

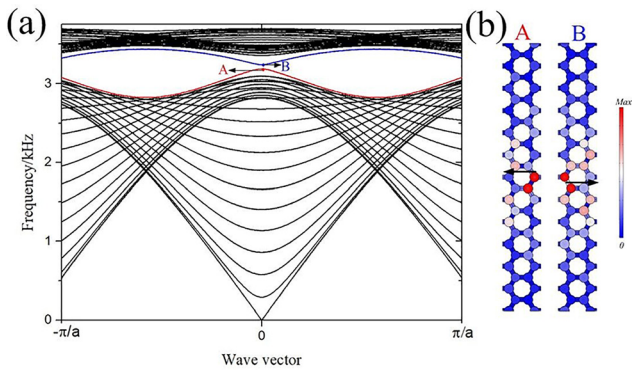


FIG. 6. (Color online) (a) Band gap structure of armchair-type interface, and (b) sound pressure distribution of valley states A and B. The figure shows the band gap structure of the armchair-type interface, in which the red and blue parts are the dispersion curves of the edge state, and the black curves represent the dispersion curves of the bulk state. The valley state is at $k = 0$ and edge states exist with a gap ranging from 3189.1 to 3238.3 Hz in the middle of the band gap of the bulk state. For this type of interface, both the K and K′ valley states appear at $k = 0$, and the band gap supports two edge states at the upper and lower cutoff frequencies. The sound pressure distribution is shown in the figure; the two edge states of sound waves propagate in the opposite directions, and the sound waves located in the edge state band gap are not transmitted across this interface.

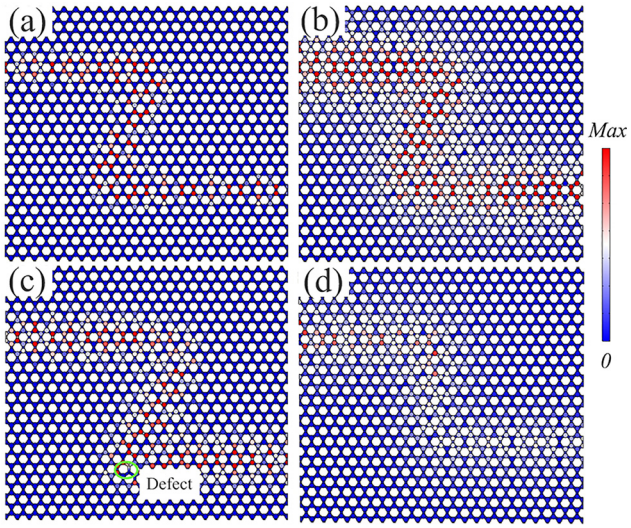


FIG. 7. (Color online) Pressure distributions of Z-shaped waveguide at (a) 3200 Hz and at (b) 3260 Hz, and (c) of Z-shaped waveguide with defect at 3260 Hz, and (d) of a rectangular waveguide at 3200 Hz.

as shown in Figs. 7(a) and 7(b). Plane waves at 3200 and 3260 Hz are applied at the left boundary around the interface, and the pressure distributions suggest that sound travels smoothly in the zigzag path despite the presence of two sharp corners. Furthermore, the sound transmission is immune to strong backscattering caused by bends in the transmission path. In addition, a defect is artificially created in the Z-shaped waveguide, as shown in Fig. 7(c), and the pressure distributions show that the sound transmission along the topological interface at valley frequencies is immune to defects. Moreover, a rectangular waveguide was established to check sound transmission along interfaces of both zigzag type (i.e., horizontal interfaces) and armchair type (i.e., vertical interfaces), as shown in Fig. 7(d). A plane wave of frequency 3200 Hz appears just inside the gap of the armchair-type edge states and stops propagating from the zigzag to the armchair interfaces. This result is consistent with the previous analysis of the band structure, and the structures allow robust transmission of acoustic waves through sub-wavelength topological edges.

## VI. CONCLUSION

This paper proposes a graphene-like structure based on a sub-wavelength resonant unit Helmholtz resonator to implement a sub-wavelength Dirac cone and produce topological phase transitions. The creation of sub-wavelength topological spin states depends on the radii of the two adjacent acoustic chambers, and these states are characterized by valley Chern numbers of opposite sign. We verified the topological valley edge states at two types of interfaces (zigzag and armchair) and found that gapless topological valley edge states appear only at zigzag interfaces, whereas gap edge states appear at armchair interfaces. Moreover, the results show that the transmission properties of edge states in a zigzag rectangular waveguide are immune to backscattering and defects.

## ACKNOWLEDGMENTS

We acknowledge project supported by the National Natural Science Foundation of China (Grant Nos. 11602269 and 11802213), the Strategic Priority Research Program of the Chinese Academy of Sciences (Grant No. XDB22040301), and the Research Program of Beijing (Grant Nos. Z161100002616034 and Z171100000817010).

Bernevig, B. A., Hughes, T. L., and Zhang, S. C. (**2006**). "Quantum spin Hall effect and topological phase transition in HgTe quantum wells," Science **314**, 1757–1761.
Fang, N., Xi, D., Xu, J., Ambati, M., Srituravanich, W., Sun, C., and Zhang, X. (**2006**). "Ultrasonic metamaterials with negative modulus," Nat. Mater. **5**, 452–456.
Fleury, R., Khanikaev, A. B., and Alù, A. (**2016**). "Floquet topological insulators for sound," Nat. Commun. **7**, 11744.
Fleury, R., Sounas, D., and Alu, A. (**2014**). "Non-reciprocal acoustic devices based on spatio-temporal angular-momentum modulation," J. Acoust. Soc. Am. **136**, 2281.
Hafezi, M., Mittal, S., Fan, J., Migdall, A., and Taylor, J. (**2013**). "Imaging topological edge states in silicon photonics," Nat. Photon. **7**, 1001–1005.
Hasan, M. Z., and Kane, C. L. (**2010**). "Colloquium: Topological insulators," Rev. Mod. Phys. **82**, 3045–3067.
He, C., Li, Z., Ni, X., Sun, X.-C., Yu, S.-Y., Lu, M.-H., Liu, X.-P., and Chen, Y.-F. (**2016**). "Topological phononic states of underwater sound based on coupled ring resonators," Appl. Phys. Lett. **108**, 031904.
He, C., Ni, X., Ge, H., Sun, X. C., Chen, Y. B., Lu, M. H., Liu, X.-P., and Chen, Y.-F. (**2015**). "Acoustic topological insulator and robust one-way sound transport," Nat. Phys. **12**, 1124–1129.
Huang, X., Lai, Y., Hang, Z. H., Zheng, H., and Chan, C. T. (**2011**). "Dirac cones induced by accidental degeneracy in photonic crystals and zero-refractive-index materials," Nat. Mater. **10**, 582–586.
Kane, C. L., and Mele, E. J. (**2005**). "Quantum spin Hall effect in graphene," Phys. Rev. Lett. **95**, 226801.
Khanikaev, A. B., Fleury, R., Mousavi, S. H., and Alù, A. (**2015**). "Topologically robust sound propagation in an angular-momentum-biased graphene-like resonator lattice," Nat. Commun. **6**, 8260.
Khanikaev, A. B., Hossein Mousavi, S., Tse, W. K., Kargarian, M., Macdonald, A. H., and Shvets, G. (**2012**). "Photonic topological insulators," Nat. Mater. **12**, 233–239.
Klitzing, K. V. (**1986**). "The quantized Hall effect," Rev. Mod. Phys. **58**, 519–531.
Laughlin, R. B. (**1983**). "Anomalous quantum Hall effect: An incompressible quantum fluid with fractionally charged excitations," Phys. Rev. Lett. **50**, 1395–1398.
Lu, J., Qiu, C., Ke, M., and Liu, Z. (**2016**). "Valley vortex states in sonic crystals," Phys. Rev. Lett. **116**, 093901.
Lu, J., Qiu, C., Ye, L., Fan, X., Ke, M., Zhang, F., and Liu, Z. (**2017**). "Observation of topological valley transport of sound in sonic crystals," Nat. Phys. **13**, 369–374.
Martin, I., Blanter, Y. M., and Morpurgo, A. F. (**2008**). "Topological confinement in bilayer graphene," Phys. Rev. Lett. **100**, 036804.
Miniaci, M., Pal, R. K., Morvan, B., and Ruzzene, M. (**2018**). "Experimental observation of topologically protected helical edge modes in patterned elastic plates," Phys. Rev. X **8**, 031074.
Mousavi, S. H., Khanikaev, A. B., and Wang, Z. (**2015**). "Topologically protected elastic waves in phononic metamaterials," Nat. Commun. **6**, 8682.
Ni, X., He, C., Sun, X. C., Lu, M. H., and Chen, Y. F. (**2016**). "Topologically protected one-way edge mode in networks of acoustic resonators with circulating air flow," New. J. Phys. **17**, 053016.
Peng, Y.-G., Qin, C.-Z., Zhao, D.-G., Shen, Y.-X., Xu, X.-Y., Bao, M., Jia, H., and Zhu, X.-F. (**2016**). "Experimental demonstration of anomalous Floquet topological insulator for sound," Nat. Commun. **7**, 13368.
Qi, X. L., and Zhang, S. C. (**2011**). "Topological insulators and superconductors," Rev. Mod. Phys. **83**, 1057–1110.
Qiao, Z., Jung, J., Niu, Q., and Macdonald, A. H. (**2011**). "Electronic highways in bilayer graphene," Nano Lett. **11**, 3453–3459.
Rechtsman, M. C., Zeuner, J. M., Plotnik, Y., Lumer, Y., Podolsky, D., Dreisow, F., Nolte, S., Segev, M., and Szameit, A. (**2013**). "Photonic Floquet topological insulators," Nature **496**, 196–200.

Semenoff, G. W., Semenoff, V., and Zhou, F. (**2008**). "Domain walls in gapped graphene," Phys. Rev. Lett. **101**, 087204.
Souslov, A., van Zuiden, B. C., Bartolo, D., and Vitelli, V. (**2017**). "Topological sound in active-liquid metamaterials," Nat. Phys. **13**(11), 1091–1094.
Wang, Z., Chong, Y., Joannopoulos, J. D., and Marin, S. (**2009**). "Observation of unidirectional backscattering-immune topological electromagnetic states," Nature **461**, 772–775.
Wei, Q., Tian, Y., Zuo, S. Y., Cheng, Y., and Liu, X. J. (**2017**). "Experimental demonstration of topologically protected efficient sound propagation in an acoustic waveguide network," Phys. Rev. B **95**, 094305.
Yang, Z., Gao, F., Shi, X., Lin, X., Gao, Z., Chong, Y., and Zhang, B. (**2015**). "Topological acoustics," Phys. Rev. Lett. **114**, 114301.
Yves, S., Fleury, R., Berthelot, T., Fink, M., Lemoult, F., and Lerosey, G. (**2017a**). "Crystalline metamaterials for topological properties at subwavelength scales," Nat. Commun. **8**, 16023.
Yves, S., Fleury, R., Lemoult, F., Fink, M., and Lerosey, G. (**2017b**). "Topological acoustic polaritons: Robust sound manipulation at the subwavelength scale," New J. Phys. **19**, 075003.
Zhang, Z., Tian, Y., Cheng, Y., Liu, X., and Christensen, J. (**2017a**). "Experimental verification of acoustic pseudospin multipoles in a symmetry-broken snowflakelike topological insulator," Phys. Rev. B **96**, 241306.
Zhang, Z., Wei, Q., Cheng, Y., Zhang, T., Wu, D., and Liu, X. (**2017b**). "Topological creation of acoustic pseudospin multipoles in a flow-free symmetry-broken metamaterial lattice," Phys. Rev. Lett. **118**, 084303.